Controllability of Voltage- and Calcium-Driven Alternans in a Cardiac Ionic Model

Laura M Muñoz[1], Mark O Ampofo[1], Elizabeth M Cherry[2,1]

[1]Rochester Institute of Technology, Rochester, NY, USA
[2]Georgia Institute of Technology, Atlanta, GA, USA

Abstract

Electrical alternans, a beat-to-beat alternation in cardiac action potential duration, can precede dangerous arrhythmias. Alternans may arise from different mechanisms, including instabilities in membrane-potential dynamics (voltage-driven alternans) or intracellular calcium dynamics (calcium-driven alternans). Some studies indicated that effectiveness of alternans suppression strategies may depend on the mechanism. We recently examined mechanistic influences on alternans controllability within a map model, but low dimensionality of the model limited the analysis to a small number of strategies. In the present work, we studied effects of different mechanisms on controllability within a higher-dimensional model, the Shiferaw, Sato, and Karma (SSK) ionic model, which allowed us to test a wider range of strategies. For voltage-driven alternans, perturbing a potassium rectifier variable was the best strategy, in terms of maximizing modal controllability of the dominant SSK alternans eigenvalue, followed by several calcium-based approaches. For calcium-driven alternans, the best strategy was to perturb intracellular Ca^{2+} concentration, but the more practical strategy of adjusting voltage was still viable for either mechanism. Controllability was more mechanistically dependent for SSK than the map model, although some SSK properties aligned with those of an ionic model studied previously.

1. Introduction

Cardiac action potentials (APs) can exhibit a beat-to-beat alternation in AP duration (APD) called alternans, which is sometimes a precursor to more dangerous abnormal rhythms [1]. Alternans may be induced by different mechanisms, including instabilities in the membrane potential dynamics (voltage-driven alternans) or intracellular calcium cycling (calcium-driven alternans) [2, 3]. Many alternans control methods have been reported in the literature, while a smaller number of studies have tested the impact of different alternans drivers on the performance of control methods (e.g., [4, 5]). Prospects for successful alternans control have in some cases appeared to depend on the mechanism [4, 5]. In a related body of work, researchers have used methods from control theory, such as controllability analysis, to determine best methods for suppressing alternans. In informal terms, controllability is a model property that indicates whether a given control method is capable of steering a system toward a desired behavior. Our recent analysis [6] of the Qu, Shiferaw, and Weiss (QSW) map model [7] was the first to combine these approaches by comparing the effects of differing alternans mechanisms on the controllability of a cardiac model.

The low dimensionality of the QSW model restricted the number of control strategies we could investigate. Hence, in the current study, we evaluated controllability of the Shiferaw, Sato, and Karma (SSK) model [8], a 16-variable ionic model that was of interest due to its ability to represent multiple alternans mechanisms. Using methods from our past work [9], we estimated eigenvalues and eigenvectors for a linearized SSK model, then computed modal controllability measures to determine best strategies for suppressing voltage- and calcium-driven alternans over a range of pacing periods. To our knowledge, the present work is the first controllability study of a cardiac ionic model that represents multiple mechanisms of alternans.

2. Methods

The dynamical equation for the SSK model may be written as $\dot{X} = f(X, I_{stim}(t))$, where the state vector is $X = [V\ m\ h\ j_{Na}\ X_r\ X_s\ X_{to}\ Y_{to}\ d\ f\ q\ c_s\ c_{int}\ c_{sr}\ c'_{jsr}\ I_{rel}]^T$. The stimulus current at time t, $I_{stim}(t)$, was a rectangular pulse train with period T, with other settings described elsewhere [5]. The state variables are membrane potential V (mV), dimensionless gating variables m, h, j_{Na}, X_r, X_s, X_{to}, Y_{to}, d, f, and q, calcium concentrations in the submembrane space (c_s), bulk myoplasm (c_{int}), and sarcoplasmic reticulum (SR) including network and junctional SR (NSR and JSR) volumes (c_{sr}), average JSR calcium concentration of compartments not being drained (c'_{jsr}), and total SR release current I_{rel} ($\mu M/s$). Calcium

concentrations have units of μM. To promote alternans, we used the voltage-driven and calcium-driven alternans SSK model parameterizations of Groenendaal et al [4]. All computations were performed in Matlab.

Fixed points were estimated, the model was numerically linearized about the fixed points, and controllability measures were computed using methods previously applied by our group to the Luo Rudy dynamic (LRd) model [10]. As an intermediate step, a discrete map form of the SSK model, $X((j+1)T) = F(X(jT))$, was produced by numerically time-integrating the ODEs over one period (from the beginning of one I_{stim} pulse to the next), where $j = 0, 1, 2, ...$ is the period index. The SSK model was integrated using an explicit Euler method together with a Rush-Larsen scheme with a time step of 0.01 ms. Fixed points $X^* = F(X^*)$ were estimated using a Newton-Krylov solver [11] for periods T in the range of 300 to 800 ms, which included the bifurcation to alternans for the parameter sets considered. State matrices (i.e., Jacobians evaluated at fixed points) $A = \partial F/\partial X|_{X*}$ were computed through central-difference numerical approximations.

After defining a deviational state vector $x_j = X_j - X^*$, controllability of the linearized dynamical system $x_{j+1} = Ax_j + Bu_j$ was examined for each of the aforementioned periods and for both alternans mechanisms. The linearized system $x_{j+1} = Ax_j$ was augmented with Bu_j, where u_j denotes the control input applied at the beginning of the j-th cycle. The input matrix B encodes the variables through which control inputs may be applied. For simplicity, it was assumed that each control strategy consisted of perturbing a single state variable every T ms. To select the i-th strategy (perturb i-th state variable only), B was set equal to B_i, defined here as the i-th column of the identity matrix.

To allow for fairer comparisons across strategies, a diagonal nondimensionalizing matrix S was computed (as per [9]) for each parameter set. A nondimensional state vector was defined as $\bar{x} = Sx$, yielding $\bar{x}_{j+1} = \bar{A}\ \bar{x}_j + \bar{B}u_j$ Here, $\bar{A} = SAS^{-1}$ and $\bar{B} = SB$. Eigenvalues λ_k and left eigenvectors $\bar{w}_k$ of $\bar{A}$ were computed using Matlab's `eig` function, for $k \in \{1, 2, ...16\}$. "Alternans" eigenvalues were defined as those with negative real part, since such eigenvalues induce beat-to-beat alternations in the response of the linearized system. λ_{alt} (or alt by itself) refers to the largest alternans eigenvalue. Here, eigenvalues are sometimes referred to as modes.

Next, the modal controllability measure of Hamdan and Nayfeh [12], $|\cos\theta_{k,i}| = |\bar{w}_k^* \cdot \bar{B}_i|/(\|\bar{w}_k^*\|\|\bar{B}_i\|)$, was computed. For the case where $\bar{A}$ has distinct eigenvalues and $|\cos\theta_{k,i}| \neq 0$, λ_k is said to be controllable (and can be reassigned to a desired location) through appropriately chosen periodic perturbations to the i-th state variable. Strategies with larger values of $|\cos\theta_{alt,i}|$ are predicted to be better able to suppress alternans.

We computed modal controllability values for a range of strategies. While the V strategy (perturbing membrane potential) can be implemented on real tissue, we acknowledge that adjusting gating and concentration variables on a beat-to-beat basis is not feasible with present technologies. However, these strategies were investigated here for the sake of completeness, and to improve our understanding of which alternans control methods are predicted to be beneficial independently of technological limitations.

3. Results and Discussion

Controllability magnitudes for all λ_k are shown in Figure 1 for both mechanisms and two strategies, V and c_{int}, where c_{int} was of interest because, aside from V, it is expected to be more accessible in a lab setting compared to the remaining SSK variables. For either mechanism, the periods at which $|\lambda_{alt}|$ crossed the stability boundary ($|\lambda| = 1$) coincided with the bifurcation-point periods reported by Cherry [5]. For voltage-driven alternans, over periods for which $|\lambda_{alt}| > 1$, perturbing c_{int} was generally a somewhat better strategy for controlling alternans compared with V perturbations, whereas the advantage of c_{int} over V was more pronounced for calcium-driven alternans. The marginal mode (near $|\lambda| = 1$) was also strongly controllable from c_{int} for either mechanism.

For all 16 control strategies ($B_1, B_2, ..., B_{16}$), modal controllability values for λ_{alt} are shown for a period of $T = 350$ ms in Table 1, along with period-averaged controllability values. Strategies are listed in decreasing order of their ability to control the largest alternans mode; values that are less negative indicate strategies that yield stronger controllability. For period-averaged rankings in columns 3–4 and 7–8, the averaging of $|\cos\theta_{alt,i}|$ values was performed over all periods for which $|\lambda_{alt}| > 1$, which corresponded to T from 300 to 360 ms for voltage-driven alternans and from 300 to 440 ms for calcium-driven alternans.

For either alternans mechanism and both cases of periods (averaged or $T = 350$ ms), the same eight strategies populated the top half of each list, albeit in different order depending on the mechanism. These top strategies included controlling the system through any calcium-related gating variable, current, or concentration, except for the submembrane concentration (c_s) and the voltage-dependent activation gate for L-type calcium (d), which appeared in the bottom half of each list. The top eight strategies also included perturbing either the activation gate of the slow component of the delayed rectifier potassium current (X_s) or the membrane potential (V). Within each mechanism, the rankings were similar across the $T = 350$ ms and period-averaged cases, which suggests that the period dependence of alternans controllability values shown in Figure 1 did not have a major impact on the rankings of strategies.

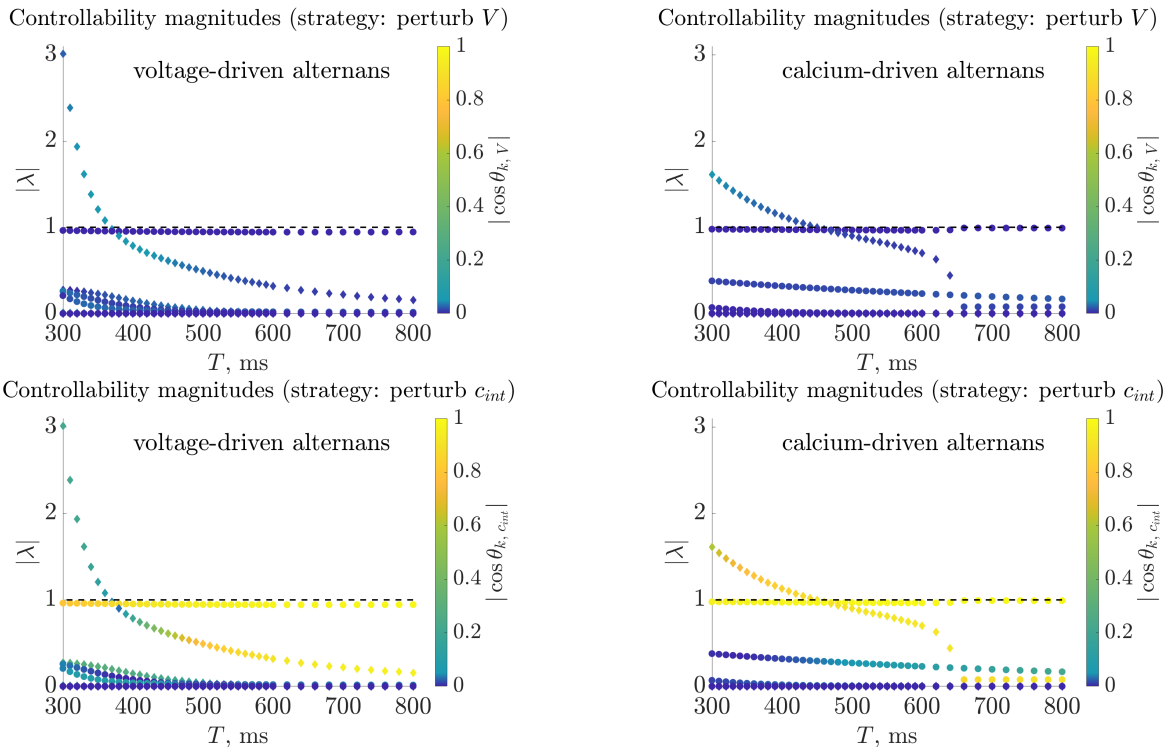

Figure 1: Modal controllability magnitudes ($|\cos\theta_{k,i}|$) of the 16 eigenvalues for each eigenvalue modulus $|\lambda_k|$ and period T, for voltage-driven (left column) and calcium-driven (right column) alternans, where the selected control strategy was to perturb V (top row) or c_{int} (bottom row). Alternans eigenvalues are labeled with diamonds, and circles indicate eigenvalues with non-negative real parts. Lighter color indicates stronger controllability. $|\lambda| = 1$ is marked with a dashed line.

Regarding the V and c_{int} strategies, Table 1 shows the largest alternans mode was more strongly controllable through perturbations to c_{int} than to V, for either mechanism. c_{int}-based control was the best strategy overall for calcium-driven alternans, while it was outranked by several other options, including X_s, which was best for voltage-driven alternans. Perturbing V yielded similar controllability magnitudes for either mechanism, although controllability of λ_{alt} from V was somewhat stronger for voltage-driven alternans.

Previously, we conducted modal controllability analyses [6, 9] of the 3-variable QSW map model and the 17-variable LRd model. For alternans suppression, the QSW model tended to favor perturbing APD over calcium-based strategies independently of alternans mechanism, which disagrees with the SSK model's ranking of several types of calcium perturbations over the V strategy. For LRd and SSK, certain calcium-based strategies were predicted to be better than V-based alternans control, and both models rank JSR-related perturbations (c'_{jsr} for SSK and total JSR Ca^{2+} concentration for LRd) very highly. In contrast with SSK results that favored c_{int} over V, LRd controllability often showed a slight preference for V over c_{int}. We examined the QSW and LRd models under a broader range of conditions than those shown in the current study, and producing a thorough comparison of controllability properties across models is a subject of ongoing work.

4. Conclusions

To gain insights on prospects for alternans suppression and the degree to which best control strategies are influenced by alternans mechanisms, a modal controllability analysis was performed on the SSK ionic model. The best strategy for suppressing alternans within the SSK model varied depending on the type of alternans, although some common strategies were indicated by the controllability measure. SSK controllability properties appeared to depend more strongly on mechanism than those reported previously for the QSW discrete map model [6]. The tendency of the SSK model to favor certain calcium-based alternans suppression methods showed partial correspondence with a past analysis of the LRd model [9].

Acknowledgments

This work was supported, in part, by the National Science Foundation under Grant Nos. CNS-1446312 and CNS-2028677.

Table 1: Control strategies ranked in decreasing strength of controllability of largest alternans eigenvalue, as quantified by base-10 logarithms (abbreviated lg) of modal controllability values, $|\cos\theta_{alt,i}|$. Columns 1–4 and 5–8 respectively show rankings for voltage- and calcium-driven alternans. Control strategies are labeled with the variable being perturbed. Controllability values are shown for both a single period ($T = 350$ ms) and averaged over all periods for which $|\lambda_{alt}| > 1$.

Voltage-Driven Alternans				Calcium-Driven Alternans			
$T = 350$ ms		Avg. over alt. periods		$T = 350$ ms		Avg. over alt. periods	
Strategy	$\lg\lvert\cos\theta_{alt,i}\rvert$	Strategy	$\lg\lvert\cos\theta_{alt,i}\rvert$	Strategy	$\lg\lvert\cos\theta_{alt,i}\rvert$	Strategy	$\lg\lvert\cos\theta_{alt,i}\rvert$
X_s	-0.195	X_s	-0.186	c_{int}	-0.114	c_{int}	-0.105
f	-0.231	f	-0.217	c'_{jsr}	-0.293	c'_{jsr}	-0.315
c'_{jsr}	-0.382	c'_{jsr}	-0.502	q	-0.555	q	-0.585
q	-0.750	q	-0.723	f	-0.612	f	-0.641
c_{int}	-0.842	c_{int}	-0.742	c_{sr}	-1.041	c_{sr}	-1.022
c_{sr}	-0.907	c_{sr}	-0.855	V	-1.485	V	-1.521
V	-1.223	V	-1.308	X_s	-1.543	X_s	-1.566
I_{rel}	-1.256	I_{rel}	-1.338	I_{rel}	-1.632	I_{rel}	-1.634
d	-2.049	Y_{to}	-1.359	Y_{t0}	-1.781	c_s	-1.781
h	-2.122	h	-1.994	c_s	-1.785	Y_{to}	-1.810
X_r	-2.251	X_r	-2.001	h	-1.834	h	-1.858
Y_{t0}	-2.378	d	-2.060	d	-2.056	d	-2.066
j_{Na}	-2.788	c_s	-2.323	X_r	-2.604	X_r	-2.630
c_s	-2.963	j_{Na}	-2.567	j_{Na}	-2.818	j_{Na}	-2.841
X_{to}	-5.346	X_{to}	-5.528	X_{to}	-7.121	X_{to}	-5.811
m	-6.974	m	-6.605	m	-16.607	m	-7.377

References

[1] Walker ML, Rosenbaum DS. Repolarization alternans: Implications for the mechanism and prevention of sudden cardiac death. Cardiovascular Research March 2003; 57(3):599–614. ISSN 00086363.

[2] Guevara M, Ward G, Shrier A, Glass L. Electrical alternans and period-doubling bifurcations. In Computers in Cardiology. 1984; 167–170.

[3] Eisner DA, Choi HS, Díaz ME, O'Neill SC, Trafford AW. Integrative analysis of calcium cycling in cardiac muscle. Circulation Research December 2000;87(12):1087–1094. ISSN 0009-7330, 1524-4571.

[4] Groenendaal W, Ortega FA, Krogh-Madsen T, Christini DJ. Voltage and calcium dynamics both underlie cellular alternans in cardiac myocytes. Biophysical Journal May 2014; 106(10):2222–2232. ISSN 00063495.

[5] Cherry EM. Distinguishing mechanisms for alternans in cardiac cells using constant-diastolic-interval pacing. Chaos An Interdisciplinary Journal of Nonlinear Science September 2017;27(9):093902. ISSN 1054-1500, 1089-7682.

[6] Muñoz LM, Ampofo MO, Cherry EM. Controllability of voltage- and calcium-driven cardiac alternans in a map model. Chaos An Interdisciplinary Journal of Nonlinear Science February 2021;31(2):023139. ISSN 1054-1500, 1089-7682.

[7] Qu Z, Shiferaw Y, Weiss JN. Nonlinear dynamics of cardiac excitation-contraction coupling: An iterated map study. Physical Review E January 2007;75(1):011927. ISSN 1539-3755, 1550-2376.

[8] Shiferaw Y, Sato D, Karma A. Coupled dynamics of voltage and calcium in paced cardiac cells. Physical Review E February 2005;71(2):021903. ISSN 1539-3755, 1550-2376.

[9] Vogt R, Guzman A, Charron C, Muñoz L. Controllability and state feedback control of a cardiac ionic cell model. Computers in Biology and Medicine 2021;139:104909. ISSN 0010-4825.

[10] Livshitz L, Rudy Y. Uniqueness and stability of action potential models during rest, pacing, and conduction using problem-solving environment. Biophysical Journal 2009; 97(5):1265–1276. ISSN 0006-3495.

[11] Kelley CT. Solving Nonlinear Equations with Newton's Method. Number 1 in Fundamentals of Algorithms. Philadelphia: SIAM, 2003.

[12] Hamdan AMA, Nayfeh AH. Measures of modal controllability and observability for first- and second-order linear systems. Journal of Guidance Control and Dynamics 1989; 12(3):421–428.

Address for correspondence:

Laura Muñoz
Rochester Institute of Technology
85 Lomb Memorial Drive, Rochester, NY, USA, 14623
laura.m.munoz@gmail.com